THE ASTROPHYSICAL JOURNAL, 457:743–751, 1996 February 1

THE DENSE CORE, OUTFLOW, AND "JET" IN L810: HIGH-RESOLUTION HAYSTACK OBSERVATIONS AT 3 MILLIMETERS

DAN P. CLEMENS
Astronomy Department, Boston University, 725 Commonwealth Avenue, Boston, MA 02215
MICHAEL BERKOVITCH
Astronomy Department, University of California at Los Angeles, Los Angeles, CA 90024
JOÃO LIN YUN
Departamento de Física, Universidade de Lisboa, Campo Grande, Edif. C1, 1700 Lisboa, Portugal
NIMESH PATEL
Harvard-Smithsonian Center for Astrophysics, 60 Garden Street, Cambridge, MA 02138
AND
TAOLING XIE
Astronomy Program, University of Maryland, College Park, MD 20742
Received 1995 April 18; accepted 1995 August 3

ABSTRACT

We have used the Haystack 37 m radio telescope to obtain high angular resolution spectral line maps of the innermost region of the star-forming Bok globule L810 (CB 205). These maps cover the central $1' \times 1'$ region with a sampling interval of 8″–10″. One map was obtained in the CO ($J = 1$–0) spectral line in order to identify the source(s) of the high-velocity gas. A CS ($J = 2$–1) map was obtained in order to find the location and kinematics of dense gas in this cloud core. Finally, a jetlike feature seen in near-infrared images was examined in two lines each of SO and SO_2, to search for postshock chemical abundance enhancements.

We find a bright 4–11 $M_\odot$ CS core associated with both the IRS near-infrared stellar source (identified by Yun et al. 1993) and the IRAS 19433+2743 far-infrared point source. The red and blue CO outflow lobes do appear to originate from IRS/IRAS 19433+2743 and join with the larger scale CO lobes mapped by Xie & Goldsmith (1990). However, the outflow lobes are not symmetrically placed about the IRS source. Instead, the outflow lobes are both offset some 30″ westward of the IRS position, producing a "swept-back" appearance. The abundance of SO is not enhanced in the region of the jetlike feature, although CS shows a local intensity maximum there. The apparent location of the near-infrared jetlike feature, in the middle of the newly resolved blue outflow lobe, may be due to either enhanced dust scattering from a preexisting cloud clump located within the outflow or it could signify the presence of a region influenced by a previous epoch of star formation within L810.

Subject headings: ISM: globules — ISM: individual (L810) — ISM: jets and outflows — ISM: structure — radio lines: ISM

1. INTRODUCTION

Star formation studies conducted toward isolated molecular clouds can be particularly revealing because of the general simplicity of the environments of many of these clouds. The L810 cloud is one such well-isolated large Bok globule, which contains the far-infrared bright point source IRAS 19433+2743, an optical reflection nebula, and a CO high-velocity bipolar outflow. However, the L810 environment may not be so simple, as a result of the relatively nearby Vulpecula OB1 association (Turner 1986). The core of this cloud has been the subject of several past investigations using a variety of observational techniques, as described below. In this paper, we report the results of a high spatial resolution spectral line mapping program, conducted at the newly upgraded Haystack telescope, aimed at resolving two outstanding questions concerning star formation in the cloud core. These questions are: (1) Given that the *IRAS* source is not located symmetrically between the CO high-velocity outflow lobes, where is the powering source of the high-velocity outflow?, and (2) Is the jetlike feature seen in the near-infrared, and which seems to point back to the *IRAS* source position, a bona fide stellar jet?

1.1. *The L810 Star Formation Laboratory*

The L810 globule ($\alpha_{2000} = 19^h45^m24^s$, $\delta_{2000} = +27°51'00''$, $l = 64°$, $b = 1°.7$. $V_{LSR} \sim 15.8$ km s^{-1}) displays modest to high optical extinction over a region of approximately $10' \times 7'$ (Clemens & Barvainis 1988), which at a distance of 2500 pc (Turner 1986; Xie & Goldsmith 1990) corresponds to a cloud core extent of about 7×5 pc.

On optical photographs (POSS) the cloud core is projected against a very dense background star field and appears to contain a small cluster of intermediate-brightness stars, as well as nebulosity seen through both red and blue filters. This central nebulosity, associated with stars projected onto the center of this cloud, makes L810 an unusually rare Bok globule.

In *IRAS* images, the globule is dominated in all bands by the bright point source IRAS 19433+2743. Some extended, much

weaker dust emission extends to the northeast of the globule core, closely following the projected distribution of a low extinction extension, or cometary tail, seen in the optical photographs.

L810 was identified as a potentially interesting star formation site by Herbst & Turner (1976), based on the presence of the central nebula, identified as a reflection nebula by its blue colors. Their optical spectroscopy and photometry of the brightest six stars in the apparent central cluster showed that all are foreground to the cloud and unrelated to the reflection nebula.

Neckel et al. (1985) probed the star-forming nature of the cloud core using deep optical photographs, long-slit optical spectroscopy, near-infrared and submillimeter photometry and centimeter wavelength radio spectroscopic and continuum mapping. Their VLA radio upper limits excluded the presence of stellar types earlier than B1, while their NH_3 and H_2CO maps revealed a dense cloud core centered on the reflection nebula and in particular on a stellar source designated star 7. Water maser emission was detected at a position west of star 7, apparently connected to that star via an Hα filament. Neckel et al. concluded that star 7 was the recently formed star responsible for the activity in the L810 core, including illuminating the reflection nebula.

Near-infrared (*H* band) polarimetry of 11 stars projected onto the core and periphery of the L810 cloud revealed evidence for ram pressure wrapping of an ambient cloud envelope magnetic field about the denser cloud core (Hodapp 1987). The field lines appear to extend from the southwest edge of the globule core (the "head") out to the low optical opacity "tail," associated with the *IRAS* dust emission zone to the northeast. This picture of an interaction of the L810 cloud with its environment provided strong additional evidence for the distance assignment of 2.5 kpc argued by Turner (1986) based on an apparent physical association with the Vulpecula OB1 stellar association.

The case for young stellar activity associated with star 7 was considerably strengthened by the results of the study conducted by Neckel & Staude (1990), in which they combined deep optical imaging photometry with optical surface polarimetry and high-dispersion long-slit spectroscopy. Strong, spectrally resolved Hα emission from star 7, as well as from another nearby star, supported the notion of activity driven by star 7. The polarimetry also showed a centrosymmetric pattern centered predominantly on star 7. Neckel & Staude further argued for the presence of a young cluster or association of some 15 embedded stars, based on the cometary appearances of their stellar images.

A CO high-velocity outflow from the cloud core was discovered by Xie & Goldsmith (1990). They found that the outflow red and blue lobes were separated along a north–south axis. This axis passed through the error ellipse for the bright far-infrared *IRAS* source, but the outflow lobes were not symmetrically placed (the *IRAS* source appeared some 20″–30″ south of the midpoint of the red and blue lobes). The relative positions of the cloud core, the outflow lobes, and the *IRAS* error ellipse are shown in Figure 1. The data shown were obtained by Yun & Clemens (1992, 1994) at the Five College Radio Astronomy Observatory (FCRAO) using the QUARRY multibeam receiver. From an LTE analysis of the Yun & Clemens FCRAO CO and ^{13}CO maps, a cloud core mass of 500 $M_\odot$ was found within 1.5 of the *IRAS* source, with at least another 250 $M_\odot$ outside that radius. A total bolometric luminosity of 890 $L_\odot$ (dominated by the bright *IRAS* point source) was established, seemingly constraining star 7 to spectral type B5 or later (Yun et al. 1993).

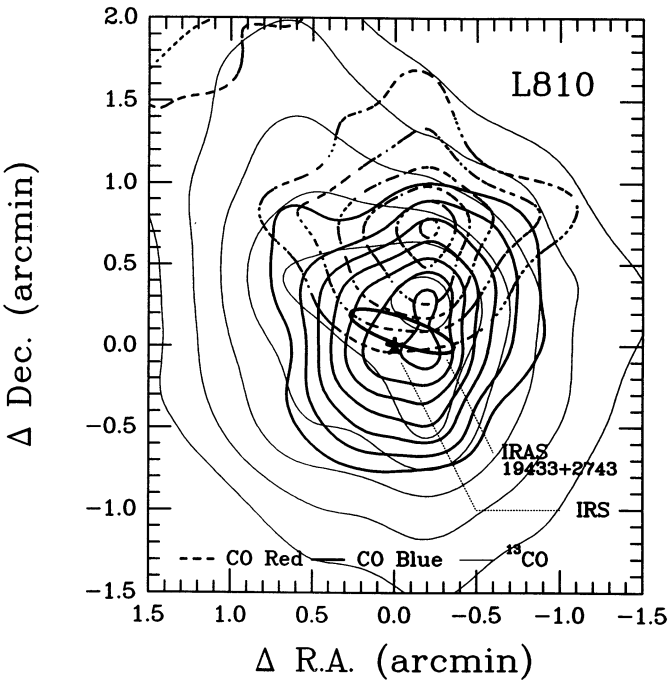

FIG. 1.—Contour maps of ^{13}CO integrated intensity (*thin, solid lines*) redshifted high-velocity CO emission (*thick, dashed lines*), and blueshifted high-velocity CO emission (*thick, solid lines*). The ^{13}CO contours begin at 6 K km s^{-1} [T_R] and are stepped by 1 K km s^{-1}. The CO red contours begin at 1 K km s^{-1} [T_R] and are stepped by 0.33 K km s^{-1}. The CO blue contours begin at 1.5 K km s^{-1} and are stepped by 0.5 K km s^{-1}. These data were obtained using the 45″ beam of the FCRAO 14 m telescope by Yun & Clemens (1994). Also shown is the 90% confidence error ellipse for the far-infrared bright point source IRAS 19433+2743, and the position of the near-infrared illuminator of the L810 reflection nebula, IRS (Yun et al. 1993).

However, Scarrott, Rolph, & Tadhunter (1991) reobserved the L810 reflection nebula under conditions of excellent seeing, using their optical imaging polarimeter. They also found a predominently centrosymmetric polarization position angle distribution, but showed that the pattern center was offset from star 7 by some 3″ to the northwest. They argued that the actual illuminator of the reflection nebula was optically invisible, but located at the polarization pattern center, and not at star 7. Further, they showed that virtually all of the light in the region, including that from the cometary stars found by Neckel & Staude, was highly polarized and due to light originating with the invisible source.

This illuminating source, named L810 IRS, was discovered at the predicted position by Yun et al. (1993), using deep near-infrared (*JHK*) imaging. The exceedingly red object IRS ([$J-K$] = 3.9 mag) was found to be symmetrically situated between the northern and southern lobes of an infrared reflection nebula which was much larger than the optical nebula found primarily southward of IRS and star 7. The near-infrared and *IRAS* fluxes were combined to yield a broadband spectral energy distribution typical of a young, class I protostar, and Yun et al. surmized that IRS was a 4 $M_\odot$ young stellar object (YSO) shining with ~10 times its eventual main-sequence luminosity.

In the near-infrared images of Yun et al. (see Fig 8, here), an elongated jetlike feature appears 30″–50″ to the southwest of

IRS. Bright knots along this feature, when linked up, point back to the IRS position, arguing for a causal relation between this feature and IRS.

But if this new feature is (due to) a stellar jet, why does it appear to be so strongly offset in position angle from the north–south CO high-velocity outflow axis seen in Figure 1? In order to try to answer this question, as well to ascertain the bona fide jet nature of this elongated near-infrared feature, we elected to use the new 3 mm high angular resolution capabilities of the Haystack telescope to probe the inner regions of the L810 cloud core. Our approach consisted of obtaining high angular resolution (8″–10″ sampled) CO and CS spectral line maps, and limited deeper integrations in two sulfur and oxygen-bearing molecular species (SO and SO_2) thought to be sensitive to shock enhancements of their abundances at stellar jet working surfaces (e.g., Pineau des Forêts et al. 1994; Chernin & Masson 1993; Chernin, Masson, & Fuller 1994).

In the sections which follow, we describe the observations and data analysis, present the maps obtained, and proceed to test the jet nature of the extended near-infrared feature. We find a less exotic explanation for the feature is most likely—namely that the feature resides along the middle of the central axis of the blue CO outflow lobe and is most probably luminous due to reflected starlight from IRS. However, the revision of the locations of the red and blue outflow axes has more substantial implications, especially regarding redirection of any true stellar jets from IRS, as described below.

2. OBSERVATIONS AND DATA PROCESSING

New observations were conducted using the 37 m Haystack radio telescope located near Westford, MA. This telescope has recently been upgraded to permit observations to be conducted at 3 mm (Barvainis et al. 1993). The spectra were collected during two periods: 1994 February 21–28 and 1994 March 16–23. The FWHM beam size was measured on the planets to be in the range 21″–18″ for observations conducted in the 98–115 GHz range, respectively. The measured main beam efficiency was typically in the range 8%–15%, depending on telescope elevation angle and observation frequency. For sources which are quite extended with respect to the main beam size, the effective coupling efficiency increases (to 32% for L810 at 115 GHz), with the fraction of the detected signal contributed by emission contained in the main beam between ~30%–50%.

The receiver employed consisted of a dual-channel SIS receiver, viewing two orthogonal linear polarizations. Including the effects of atmospheric emission and loss, the single-sideband system temperatures ranged from 200 K (at 98 GHz) to 700 K or more (115 GHz), depending on elevation angle. Spectroscopy was accomplished using two 5120 channel autocorrelator spectrometers. The total spectrometer bandwidths employed were either 53 MHz (CO outflow mapping) or 17.7 MHz (all others).

All spectra were collected in frequency-switching mode, with the offset frequency selected to be a multiple of 12.5 MHz, to reduce standing wave ripple from within the radome, and the center frequencies were selected to keep the two frequency-switched component lines within the total autocorrelator bandpass, to allow spectrum folding.

The Haystack telescope, when operated in the 3 mm band, has a strongly modulated curve of gain with elevation angle, with maximum forward gain occurring in the 30°–40° elevation angle range, and with significant loss of gain below angles of 20° and above 55°. The gain curve was established empirically by observing the apparent brightness of the 86 GHz SiO maser R Leo as a function of elevation angle (Barvainis et al. 1993), and scaling the observed gain appropriately for frequencies away from 86 GHz. While this gain curve is most appropriate for point sources, we found little deviation away from the curve for the observations of L810, and adopted the R Leo gain curve for data scaling purposes.

The short time tracks during which a particular source could be observed with optimal gain (rising, or setting, but not during transit of high declination sources) plus the relatively low main beam efficiency led to a data collection mode consisting of the construction of many short integration multiposition maps. Each map was fully observed during any one rise or set of the source, with many such maps produced during the observing runs. Each map was performed with identical setups, including pointing (performed toward H_2O masers at 22 GHz using another receiver which simultaneously viewed the sky from a fixed angular offset relative to the 3 mm optical axis) and calibration observations. All maps were independently processed and examined. Maps with obvious problems (there were several severe snow storms during the course of these observing runs) were rejected. The remaining maps were averaged, using weighting by the inverse square of the baseline noise in the constituent spectra, to produce the final maps.

2.1. CO *Maps*

The $J = 1$–0, 115 GHz line of CO was observed toward a total of 49 positions, in the form of a 7 × 7 grid about the IRS position ($\alpha_{2000} = 19^h45^m24^s.12$, $\delta_{2000} = +27°51'01''.3$). Spacing between positions was 8″.3, or half the FHWM beam size. Total integration times in each of the final spectra averaged 16 minutes. The final spectra were baselined, folded, and smoothed to 0.2 km s^{-1} spectral resolution. In these spectra, the mean rms baseline noise was 0.1 K [T_A^*].

The map-averaged mean CO line profile [T_R] for the 1 × 1 arcmin^2 region mapped is shown at the top of Figure 2. In addition to the main core of the line, whose FWHM width is about 3.5 km s^{-1}, the presence of significant red-shifted and blueshifted emitting gas can be seen. The red emission extends to about 22 km s^{-1}, while the blue emission is seen to about 9 km s^{-1}. The single CO line profile [T_R] obtained at the FCRAO (with a 45″ beam size) toward the IRS position by Yun & Clemens (1994) using a coarser spectrometer is shown in the bottom portion of Figure 2. The ratios of the line peaks and integrated intensities of the raw scans (on the T_A^* scale) were both 45%, and both showed similar red and blue wing shapes. These ratios implied that scaling of the measured value of η_{fss} for FCRAO of 70% to Haystack would yield a minimum efficiency of 32% for conversion of observed antenna temperatures [T_A^*] to radiation (brightness) temperatures [T_R] for the new data, and these ratios were used to produce the spectral comparison shown in Figure 2.

The Haystack and FCRAO CO line center intensities were established via Gaussian fitting, then converted to kinetic temperature via the assumptions of optical thickness and thermalization, resulting in the maps shown in Figure 3. That figure shows the larger scale CO-traced gas kinetic temperature from the FCRAO QUARRY data of Yun & Clemens (1994), compared to the smaller region probed using Haystack. The CO-traced gas temperature is not uniform across the face of the cloud, as is often seen toward dark clouds, but instead shows a

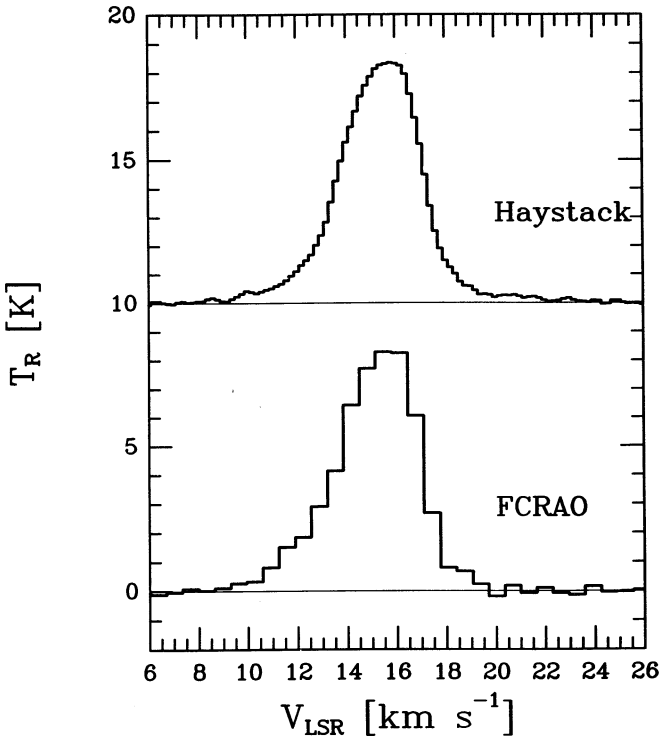

FIG. 2.—Comparison of Haystack map averaged CO spectrum (*top*) and FCRAO single position spectrum (*bottom*) both centered on IRS. Both spectra were placed on the T_R scale using efficiencies of 32% and 70%, respectively.

strong peak of up to 13 K at the IRS position, indicating localized heating of the gas by the young star in this cloud core.

The spatial distributions of the high-velocity CO emission were established using the Haystack spectra via mapping the integrated line intensity found across velocity intervals which were redshifted and blueshifted with respect to the line center velocity. Following Xie & Goldsmith (1990) and Yun & Clemens (1992, 1994), redshifted CO high-velocity emission was mapped corresponding to the LSR velocity interval 18–22 km s^{-1}, and blueshifted emission corresponding to the 9–13 km s^{-1} interval. Significant emission of both redshifted and blueshifted high-velocity gas was found across the entire Haystack map and is likely due to emission from outside the main beam (as noted above).

Figure 4 shows the spatial distributions of the *brightest* 50% of the emission seen at Haystack in the red (left) and blue (right) high-velocity intervals. Two structures are seen, which are not fully delineated by the limited angular extent of these maps. There is a region to the northwest of IRS in which the brightest redshifted CO emission (integrated intensity greater than 2 K km s^{-1} [T_R]) dominates. There is a region to the southwest of IRS in which the brightest blueshifted CO emission (brighter than 3 K km s^{-1} [T_R]) dominates. If the line integral velocity limits are moved to include only the highest velocity gas (20–22 km s^{-1} for the red, 9–11 km s^{-1} for the blue), the resulting maps look very similar to the ones shown; that is, the most extreme velocities map into the brightest high-velocity emission regions.

2.2. CS *Maps*

The $J = 2$–1, 98 GHz line of CS was observed toward a total of 25 positions, in the form of a 5 × 5 grid about the IRS

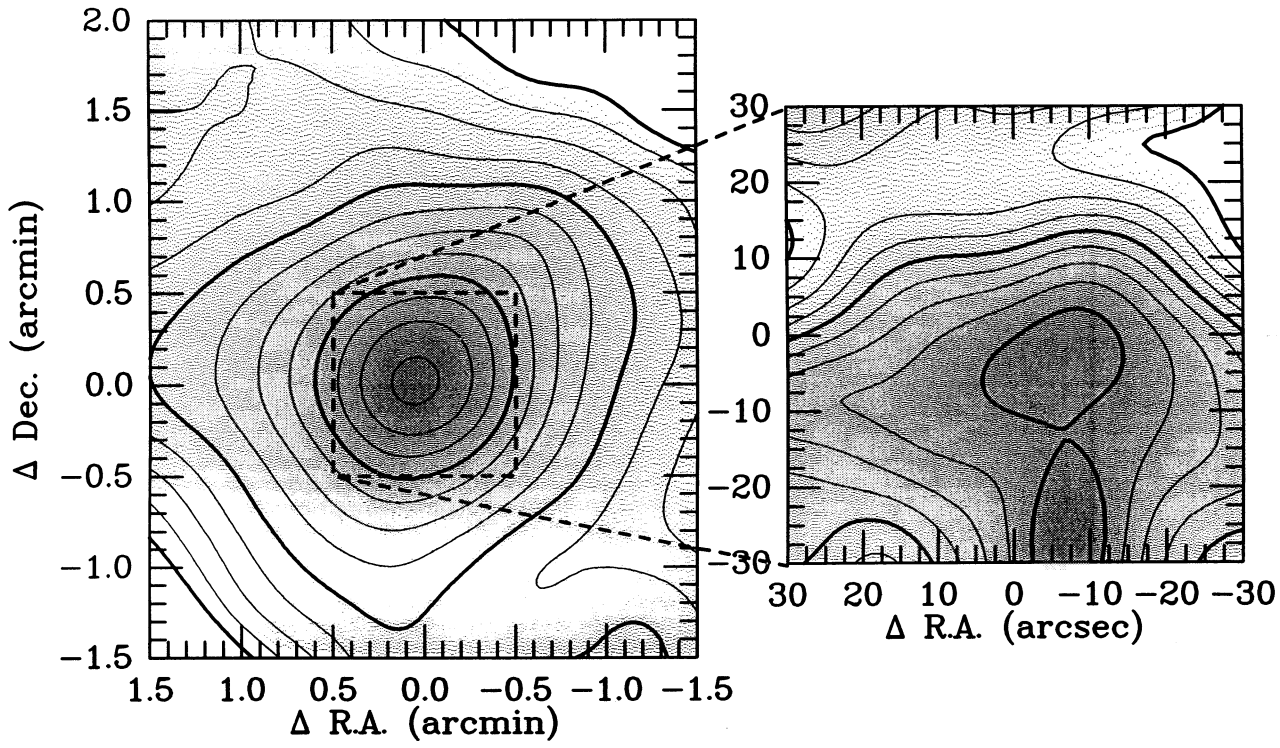

FIG. 3.—Comparison of CO traced gas kinetic temperature (excitation temperature). *Left*—FCRAO map: Contours begin at 9 K; bold contours are stepped by 1 K, thin contours by 0.25 K. *Right*—Haystack map: Lowest contour (bold) starts at 11 K, with same steps as FCRAO map.

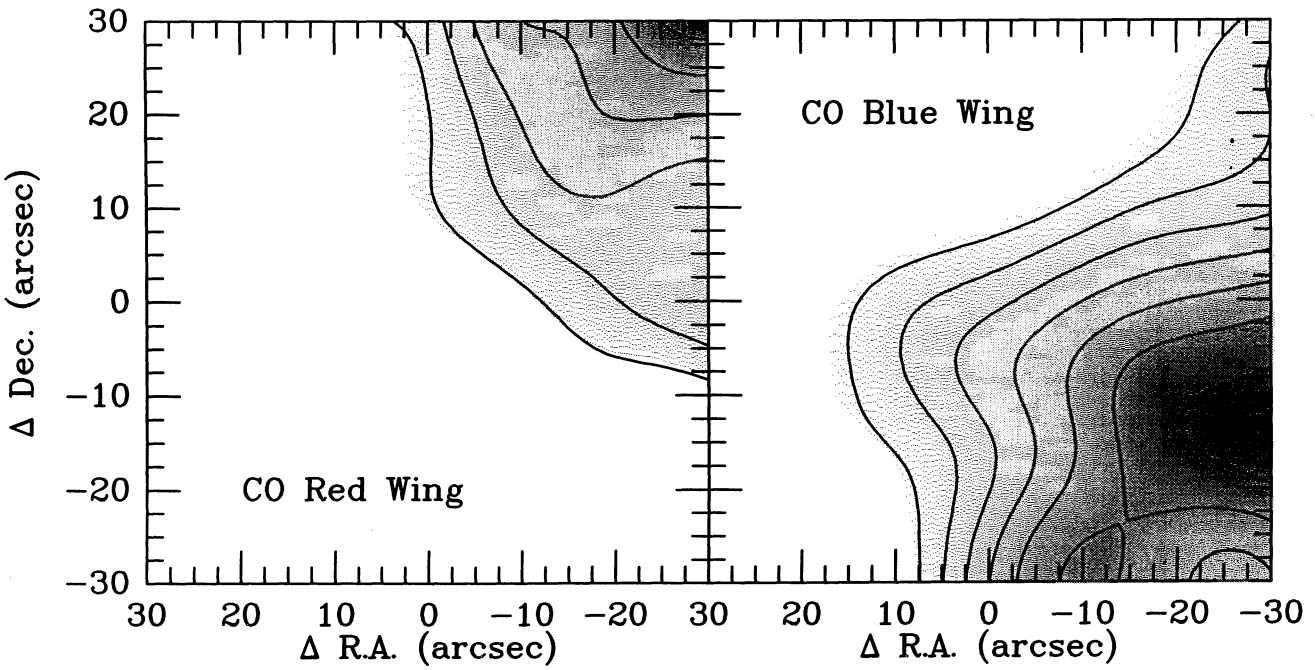

FIG. 4.—Haystack maps of the spatial distribution of the brightest 50% of the red (18–22 km s^{-1} V_{LSR}) and blueshifted (9 to 13 km s^{-1}) high-velocity emission. The redshifted emission (*left*) has a lowest contour corresponding to the mean value of the red high-velocity emission (2 K km s^{-1} [T_R], or roughly 7 times the expected noise in this velocity interval), and a contour step size of 0.6 K km s^{-1}, or 3 σ. The blueshifted emission (*right*) also begins at the 50% level (3 K km s^{-1}, or more than 10 σ) and is stepped by the same value as for the red emission.

position, in order to search for high-density gas. The spacing between positions was 9″.8, or half the FWHM beam size. Total integration times in each of the final spectra averaged 12 minutes. The final spectra were smoothed to a spectral resolution of 0.16 km s^{-1} per channel and the mean baseline noise level of the set of CS spectra was 47 mK [T_A^*] per channel.

The map-averaged CS line profile is shown at the top of Figure 5. High-velocity wings are not present, and the FWHM of the line shown is 1.7 km s^{-1}.

The spatial distribution of the integrated CS line intensity is shown as Figure 6. There was significant CS emission detected at all positions mapped at Haystack. However, the strongest emission is confined to a small structure centered on the IRS position, which is mostly resolved. For the gas kinetic temperature distribution shown in Figure 3, the optical depth of CS was computed from Gaussian fits to the line profiles, and the integrated CS line intensity used to infer the CS column density assuming LTE, with the CS excitation temperature set to the CO traced gas temperature. The peak CS column density thus found is about 1.0×10^{13} cm^{-2} at the position of IRS. This is to be compared to the ^{13}CO column density of 6.4×10^{15} also toward IRS, obtained from the FCRAO data, also assuming LTE. For a ^{13}CO to H_2 relative abundance of 2×10^{-6}, the corresponding CS abundance is 3.3×10^{-9}, similar to values found in the literature (Irvine et al. 1987; Blake 1988). Assuming this relative abundance, the total CS traced mass in the Haystack map is found to be 11 $M_\odot$, with the small region of enhanced CS emission surrounding (within 10″ of) IRS accounting for 4 $M_\odot$. The LTE conditions are probably not exactly met in this cloud core; hence absolute uncertainty levels of 50% are likely. Relative uncertainties (position-to-position for the same molecule, or molecule-to-

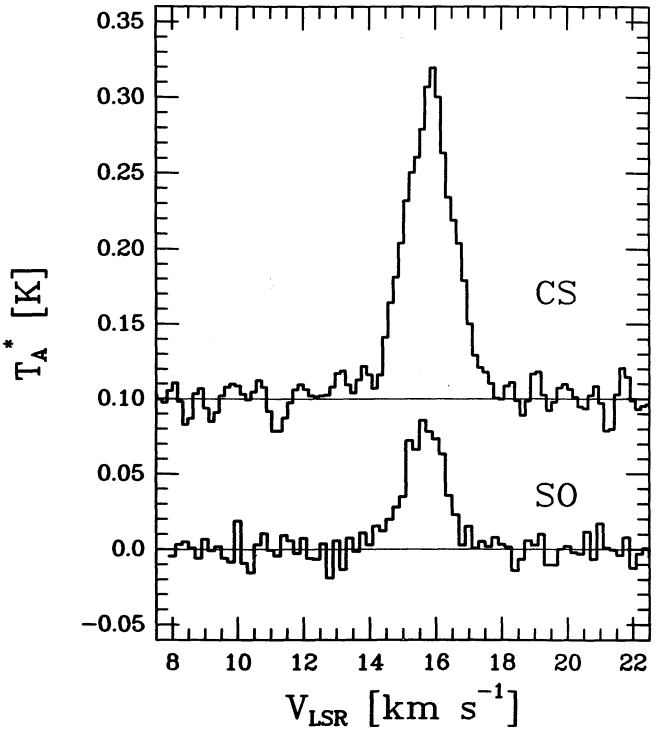

FIG. 5.—Haystack map averaged CS spectrum [T_A^*] and SO spectrum toward the L810 cloud core.

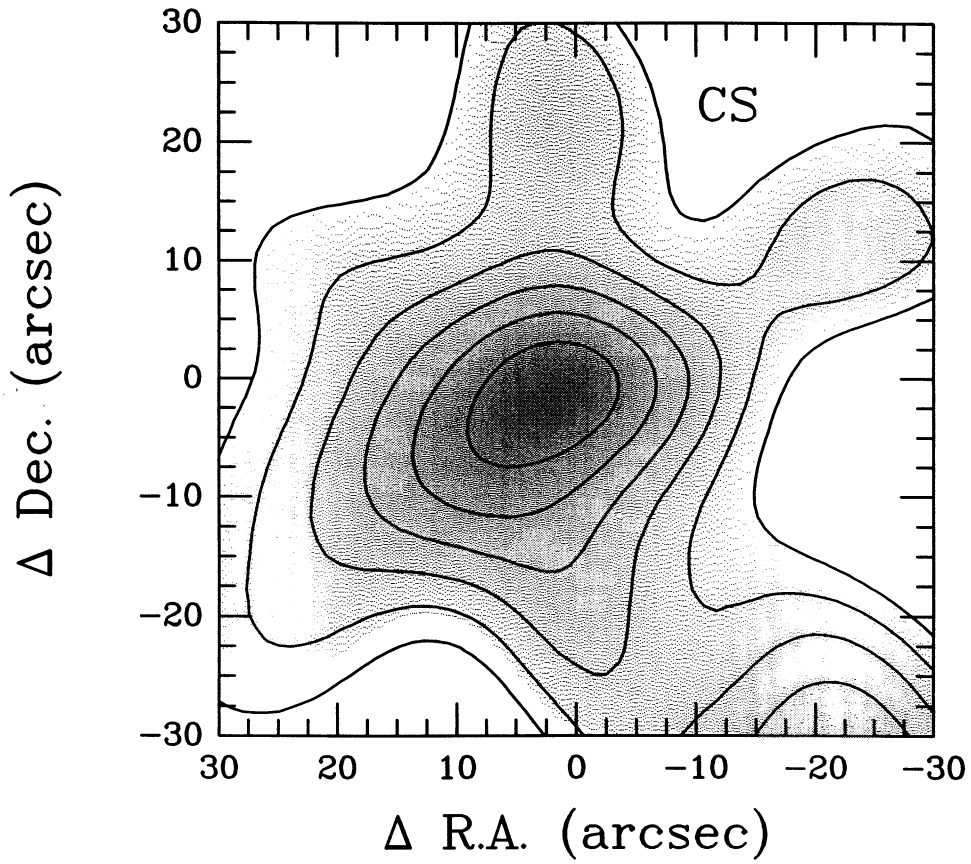

FIG. 6.—Distribution of Haystack mapped CS emission toward the L810 cloud core. Shown are contours representing integrated intensity. The first contour represents 0.2 K km s^{-1} [T_A^*], approximately 7.5 σ above zero emission, or about 1 σ above a uniform background of CS emission, with contour steps of 40 mK km s^{-1} (1 σ).

molecule at a fixed cloud position) are expected to be substantially smaller.

There are also three fainter CS features worth noting, as seen in Figure 6. The first is located in the southwest corner, corresponding to the blue CO lobe saddle point (see Fig. 4). The other two CS features, one directly north of the IRS and one to the northwest of IRS, appear to border or contain the red CO lobe emission of Figure 4. All of these features are significantly detected at greater than 8.5 σ in integrated intensity above zero intensity. However, this corresponds to only $\sim$2–3 σ above a mostly uniform CS background of $\sim$0.3 K km s^{-1} likely produced by the telescope sidelobe response.

A detectable velocity gradient is present in the central CS emission structure, of value approximately 0.4 km s^{-1} per 0.4 of offset, or about 1.4 km s^{-1} per pc. The direction of the gradient indicates an approximate rotation axis along a position angle of $\sim -20°$. If this gas is bound to a central stellar source, the binding mass required is at least 1.3 $M_\odot$. This value is consistent with the photometric estimate of about 4 $M_\odot$ for IRS (Yun et al. 1993). Thus, this 4 $M_\odot$ CS structure could be a remnant protostellar envelope left over from the formation of IRS.

2.3. SO *and* SO_2 *Observations*

Shock-enhanced abundances of sulfur and oxygen-bearing molecular species have been predicted (Pineau des Forêts et al. 1994) and detected in the vicinities of some stellar jet terminator regions (Chernin & Masson 1993; Chernin et al. 1994). Detection of such molecular abundance enhancements toward the near-infrared jet-feature seen in the Yun et al. (1993) images would be strong evidence for a true stellar jet.

A five-position SO ($J_K = 3_2$–2_1; 99.3 GHz) strip map was made along the axis connecting IRS to the jet feature. A shorter three-position strip map was also made perpendicular to that axis through the position of the infrared-brightest part of the jet feature (that associated with star 12–see Fig. 8). The SO spectra (again, obtained on several days using identical techniques) were averaged by position, smoothed to 0.2 km s^{-1} per channel spectral resolution, yielding a mean baseline noise of 20 mK [T_A^*] per channel per position. The position averaged SO spectrum for all positions observed is shown at the bottom of Figure 5.

The integrated SO emission across the 14–18 km s^{-1} velocity interval is strongest at the position of IRS (of value 0.17 ± 0.02 K km s^{-1} [T_A^*]), indicating that this molecule is sensitive to the same high-density gas which excites the CS emission. Assuming thermalization at the same excitation temperature as seen by CO, the inferred SO column density (LTE) toward IRS is 4.9×10^{12} cm^{-2}, yielding a SO relative abundance ot H_2 of 1.5×10^{-9}, fairly typical for molecular clouds (Irvine et al. 1987; Blake 1988). The SO emission is somewhat weaker at the location of the jet feature and remains weak as positional offset from IRS increases.

In order to test for an abundance enhancement of SO associated with the jet-feature position, ratios of the SO integrated line intensity relative to the CS integrated line intensity (which

is not expected to be enhanced—Pineau des Forêts et al. 1994) were computed for positions overlapping to within a half beamwidth. The mean ratio is 0.33, with no positions deviating by more than twice the propagated uncertainty (0.06) from the mean value. We conclude that SO, as traced in the $J_K = 3_2$–2_1 line, exhibits no detectable abundance enhancement associated with the jet-feature location.

In order to attempt to determine some of the gas physical conditions (temperature, volume density) present in the jet feature, very deep integrations in the $J_K = 2_3$–1_2 (109.3 GHz) line of SO and the $J_{K-1,K_1} = 3_{1,3}$–$2_{0,2}$ and $10_{1,9}$–$10_{0,10}$ (104 and 104.2 GHz) lines of SO_2 were performed toward two positions, one associated with the (star 12) near-infrared brightest portion of the jetlike feature, and one reference position located 30″ away from the first (and away from the IRS-jet axis). None of these three lines was significantly detected at either position to integrated line intensity limits (3 σ) of 0.17 (SO $3_{1,3}$–$2_{0,2}$), 0.06 (SO_2 $3_{1,3}$–$2_{0,2}$), and 0.07 (SO_2 $10_{1,9}$–$10_{0,10}$) K km s^{-1} [T_A^*].

If the SO-bearing gas was significantly clumped, or underfilled the Haystack beam, our column density estimates would represent beam-averaged lower limits to the true values, and could mask modest shock enhancements. Similarly, if low gas volume densities were to produce strongly subthermal excitation of the SO energy levels, the SO abundance could have been underestimated. However, we see no detectable SO enhancement toward the jet feature, nor along the IRS feature axis (via comparison with off-axis positions). We also see the mostly monotonic decrease in SO intensity with projected offset from IRS expected of a centrally condensed dense cloud core. We conclude that neither beam underfilling nor subthermal excitation will seriously impact our conclusions regarding either the CS or SO observations.

3. DISCUSSION

3.1. *Comparison of* CS *and* CO *Morphologies*

The relative distributions of the dense gas, as traced by CS, and the high-velocity outflowing gas, as traced by the CO line wings emission, are shown in Figure 7. In this figure, the CS core location in the map center and the offset locations of the red and blue CO high-velocity gas are indications that the activity center is associated with the star 7–IRS region. However, the high-velocity outflow from either star 7 or IRS, if initially bipolar, has been redirected into an apparent "swept-back" morphology within 5″–10″ of the jet origin. The brightest, central CS feature is weakly elongated, with a major axis along a position angle of roughly 120°.

There are interesting anticoincidences of CS and CO emission at some of the previously discussed locations in this map. These include the region just north of IRS, at offset ($\Delta\alpha$, $\Delta\delta$) = (0, 20), where a faint CS feature occurs near the edge of the red outflow lobe, and a similar region just south of IRS, at (0, −15), where the blue CO lobe suffers a local weakening (seen as a kink in the bold contours). Two other CS features are present, one in the upper right region, at (−20, 10), associated

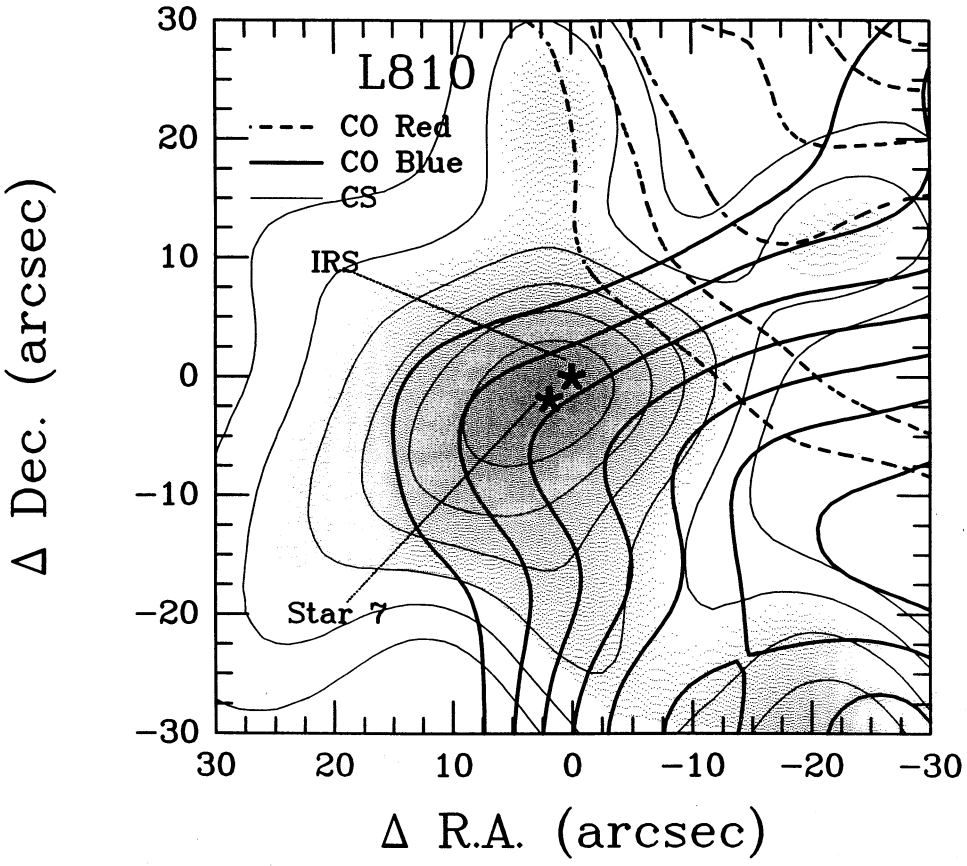

FIG. 7.—Comparison of CS integrated intensity distribution (*thin contours and halftone shading*) with the distributions of redshifted (*bold, dashed*) and blueshifted (*bold, solid*) CO high-velocity emission. The locations of the star 7 and IRS sources are indicated by a small star symbols. Contour levels are as in Figs. 4 and 6.

with a region of decreased red CO emission, and in the lower right, at (−23, −28), where a CS feature is very close to the CO blue wing saddle point at (−15, −25).

One possible physical explanation is that these weak CS features represent denser, or more highly excited interfaces (walls) between the mostly evacuated outflow lobes and the ambient cloud core. The anticoincidence of the CS and CO would then be a natural consequence of the CS cavity walls serving to confine (or act as the physical source of) most of the high-velocity CO emitting gas. This would explain the locations of three of the four faint CS features as appearing near the outer boundaries of the CO lobes.

The fourth CS feature, in the southwest corner, seems to be located very close to the central axis running from IRS along the center of the blue CO lobe. In the following section, this CS feature is shown to correspond almostly exactly to the region of strongest near-infrared emission associated with star 12 within the jetlike feature.

3.2. *Comparison of* 3 mm *and Near-Infrared Morphologies*

When the CS integrated intensity distribution is overplotted on the near-infrared *K*-band image, the relationship between dense gas, outflowing gas, and the jetlike feature becomes clearer, as shown in Figure 8.

In this figure, the central CS emission appears elongated with a direction almost exactly parallel to the star 7–IRS axis (position angle 135°). The central, near-infrared bright portion of the embedded reflection nebula is well covered by the central CS emission, offering an explanation for the origin of the extinction to the star 7–IRS region.

The near-infrared "jet" features corresponds to one of the weaker CS emitting regions. The "jet" and the CS region are both located in the middle of the blue CO outflow lobe (see Fig. 7).

In the region occupied by the red CO high-velocity lobe (the northwest corner), the CS emission appears to be anti-correlated with some of the diffuse infrared emission. This likely indicates that this diffuse infrared arises from scattering off the embedded back (or front) side(s) of the evacuated red outflow cavity. In that case, the scattering will most likely be single in nature, with high polarizations expected for this infrared emission (Whitney & Hartmann 1993).

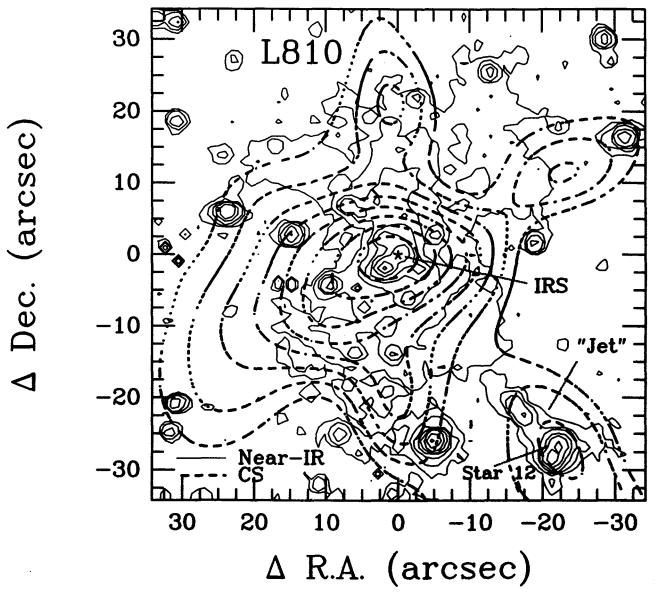

FIG. 8.—Comparison of CS integrated intensity distribution (*bold, dashed contours*), with near-infrared *K*-band intensity (*thin, solid contours*; from Yun et al. 1993). The IRS, star 12, and "jet" features are identified on the figure.

3.3. *One Comprehensive Scenario, Two Interpretations*

From the new Haystack observations, and especially when combined with the near-infrared images, a detailed picture or scenario of the L810 cloud core may be developed. The key features include: at least one protostar, identified by Scarrott et al. (1991) and Yun et al. (1993) not as star 7 but as the IRS object; a remnant dense cloud core (seen in CS); a bipolar protostellar jet (*not* yet directly seen); a mechanism for redirecting that jet within 5″–10″ of the protostar; a redshifted outflow lobe directed toward the northwest, deeply embedded in the cloud, confined by dense or warm ambient cloud material (the weak CS features); a blueshifted outflow lobe directed toward the southwest, and toward the front surface of the cloud, confined along its southern boundary (by another CS feature); and, finally, a small region of dense gas located in, or projection onto, the center of the blue outflow lobe (the jet-feature plus one faint CS feature).

There are two major questions left open by this scenario. The first involves the nature of the redirection of the protostellar jet outflow. Such redirection is exceedingly unusual and would seem to require another agent, perhaps ram pressure, perhaps relative cloud–protostar motion. We believe that the possible interaction of a wind from star 7 (which is also likely to be fairly young) with the true stellar jets from IRS could be the redirecting agent, but cannot test this notion using the current data.

The second question involves the exact nature of the near-infrared jetlike feature. We have shown in this work that this feature is not directed along some unusual direction relative to the outflowing gas, as was concluded from a comparison of the near-infrared images with the lower angular resolution FCRAO CO high-velocity maps. Instead, this feature is clearly placed in the center of the blueshifted outflow. The lack of detectable elevated SO or SO_2 abundances may argue against the shock enhancements predicted by Pineau des Forêts et al. (1994). However, not every jet terminator shows such enhancements (Chernin et al. 1994), so the absence of detectable enhancement cannot alone preclude a true jet interpretation.

There are at least two possible alternative explanations for the apparent jetlike feature. In the first, a preexisting dense clump of gas and dust in the ambient cloud becomes uncovered by the action of the protostellar jet and outflowing gas, but does not erode as quickly as any less dense gas in the vicinity. Such a dense region could represent a condensing clump which failed to accumulate sufficient gas to form a star before the initiation of an interaction with the IRS outflow. In this scenario, the near-infrared light seen would most likely arise from single scattering of IRS light by the now eroding surface of the failed dense clump. The shape of the "jet" feature in the near-infrared, especially the lower surface brightness "tongue" pointing back to IRS, could represent either growth of a Rayleigh-Taylor instability, or stagnation or back flow of the IRS driven gas. Note that this feature shows up as a saddle point in the CO outflow maps, possibly due to complex, non-laminar outflow velocities or directions there.

Troubling to this explanation are the surface polarimetric observations of Scarrott et al. (1991). At an offset of (−21,

−28) an optically visible star, star 12 (a late B dwarf, according to Neckel & Staude), is seen (as noted in Fig. 8). This optical star corresponds to the southern of the two near-infrared peaks in the brightest portion of the "jet" feature. In their polarimetric maps, the region within 2″–3″ of star 12 is illuminated by star 12 and is not shining due to the scattering of light emitted by IRS (as is all the nebulous emission beyond 3″ from star 12). Scarrott et al. concluded that star 12 is located either within the front surface of the molecular cloud or is foreground but near to the cloud surface, and illuminates a portion of the cloud via backscattering. This would seem to place part of the near-infrared "jet" feature very close to the cloud surface. However, this should make it less likely to be associated with a region of dense gas, since such regions tend to be deeply embedded in cloud centers.

However, Neckel & Staude (1990) estimated the extinction to star 12 to be almost 6 mag at V band. This is similar to the 7 mag to star 7, but much less than the more than 15 mag required to explain the very red spectral energy distribution of IRS (Yun et al. 1993). Six magnitudes of extinction to star 12 is inconsistent with a location near the front surface of the cloud.

If star 12, the near-infrared "jet," and the CS feature are all related, then the explanation consisting of a preexisting, starless, dense gas clump is weakened.

A second possibility is that star 12, and indeed its near-infrared companion (the second peak in the near-infrared "jet" feature, located 1.″5 to the northwest of star 12, shows up prominently in narrow band 2.12 μm images taken under conditions of subarcsecond seeing—Yun 1995), represent an earlier epoch of star formation in the L810 cloud core. Bounding timescales for such an epoch would include a lower limit of a few hundred thousand years, based on the dynamical age of the IRS red outflow lobe, and an upper limit of a few million years, based on the main-sequence lifetime for a late B dwarf star. Under this scenario, the direction of the action is somewhat reversed, with a strong jet from star 12 (or its red companion) having carved out the current zone occupied by the blue outflow from IRS, and perhaps the star 7–IRS star formation triggered by the outflow activity associated with the star system. At the current epoch, some dense gas and dust could still be associated with the star 12 system and illuminated by star 12. The apparently fortuitous location of this system within the IRS blue outflow lobe would then represent no accident, but the appropriation of the existing low-density (star 12) cavity by the new IRS outflow. Disruption of the IRS blue outflow in the vicinity of the star 12 system would also be a natural consequence.

4. SUMMARY

The newly commissioned 3 mm capabilities of the Haystack telescope were used to obtain high angular resolution (sampling interval of 8″–10″) two-dimensional spectral line maps in CO, CS, and a strip map in SO of the central 1′ region of the L810 molecular, centered on the star 7–IRS stellar pair. This structure shows velocity shear consistent with rotation about a minimum mass of 1.3 $M_\odot$. The CO maps showed high-velocity red and blueshifted gas distributions which appear offset, or "swept back" from IRS, while still most likely driven by IRS. The CS and CO maps of line emission show the anticorrelations expected of dense, warm ambient cloud gas defining outflow lobe cavity walls containing lower density, but much warmer outflowing gas. The near-infrared "jet" feature was found to be associated with a minor CS enhancement and the central axis of the blue CO outflow lobe. SO, though detected, was not found to be enhanced in the vicinity of the "jet" feature. A second line of SO, and two lines of SO_2 were not detected toward either the "jet" or a reference position.

Activity in the L810 cloud core appears to be currently driven by the deeply embedded IRS source. However, the required redirection of the outflow within 5″–10″ of IRS is not currently explained, though some interaction with the nearby star 7 seems most likely.

The near-infrared "jet" feature is not necessarily a bona fide jet from IRS. Instead it may represent an as yet uneroded dense gas and dust clump uncovered by and contained within the IRS blue outflow lobe. Alternatively, the association of this near-infrared feature with the optical star 12 system, which possesses its own reflection nebula and is modestly embedded in the cloud, could signify the location of a previous epoch of star formation within L810.

We wish to thank the Haystack staff for their important and crucial assistance in this investigation. Careful readings and constructive comments on the manuscript by the referees were also appreciated. This work was partially supported by NSF grant AST 92-21194 and NSF REU supplement -01 to D. C.

REFERENCES

Barvainis, R., Ball, J. A., Ingalls, R. P., & Salah, J. E. 1993, PASP, 105, 1334.
Blake, G. A. 1988, in Molecular Clouds in the Milky Way and External Galaxies, ed. R. L. Dickman, R. L. Snell, & J. S. Young (New York: Springer-Verlag), 132
Chernin, L., & Masson, C. 1993, ApJ, 403, L21
Chernin, L. M., Masson, C. R., & Fuller, G. A. 1994, ApJ, 436, 741
Clemens, D. P., & Barvainis, R. 1988, ApJS, 68, 257
Herbst, W., & Turner, D. G. 1976, PASP, 88, 308
Hodapp, K.-W. 1987, ApJ, 319, 842
Irvine, W. M., Goldsmith, P. F., & Hjalmarson, Å. 1987, in Interstellar Processes, ed. D. Hollenback & H. Thronson (Dordrecht: Reidel), 561
Neckel, T., Chini, R., Güsten, R., & Wink, J. E. 1985, A&A, 153, 253
Neckel, T., & Staude, H. J. 1990, A&A, 231, 165
Pineau des Forêts, G., Roueff, E., Shilke, P., & Flower, D. R. 1994, MNRAS, 262, 915
Scarrott, S. M., Rolph, C. D., & Tadhunter, C. N. 1991, MNRAS, 248, 27
Turner, D. G. 1986, A&A, 167, 157
Whitney, B. A., & Hartmann, L. 1993, ApJ, 402, 605
Xie, T., & Goldsmith, P. F. 1990, ApJ, 359, 378
Yun, J. L., Clemens, D. P. 1992, ApJ, 385, L21
———. 1994, ApJS, 92, 145
Yun, J. L., Clemens, D. P., McCaughrean, M. J., & Rieke, M. 1993, ApJ, 408, L101
Yun, J. L. 1995, private communication